Theory of strain tunning exction coupling in self-assembled InAs/GaAs quantum dots

Jianping Wang,[1,2] Guang-Can Guo,[1,2] and Lixin He[1,2,*]

[1] *Key Laboratory of Quantum Information, University of Science and Technology of China, Hefei, 230026, China*
[2] *Synergetic Innovation Center of Quantum Information and Quantum Physics, University of Science and Technology of China, Hefei, 230026, China*

(Dated: February 28, 2024)

We derive analytically the change of exciton fine structure splitting (FSS) under the external stresses in the self-assembled InAs/GaAs quantum dots using the Bir-Pikus model. We find that the FSS change is mainly due to the strain induced valence bands mixing and valence-conduction band coupling. The exciton polarization angle under strain are determined by the argument of the electron-hole off-diagonal exchange integrals. The theory agrees well with the empirical pseudopotential calculations.

PACS numbers: 73.21.La, 78.67.Hc, 42.50.-p

arXiv:1401.2695v1 [cond-mat.mtrl-sci] 13 Jan 2014

I. INTRODUCTION

Self-assembled quantum dots (QDs), also known as artificial atoms, are made of millions of atoms.[1] Unlike real atoms, which have constant physical properties, the QDs are different from each other and show far more complicate behavior. The physical properties of QDs, are determined by the combined effects of the strain distributions, alloy, interface etc., which are coined during their growing process. It is a great challenge, as well as an opportunity, to tune the QDs to desired properties (e.g., the exciton energy, polarization, and fine structure splitting etc.) by external fields, which is not only interesting for fundamental physics, but is also extremely important for device applications. However, despite the importance, our understanding to the interplay between the QDs and external fields is still very limited.

One of the most prominent applications of QDs is as the entangled photon emitters, based on the biexciton cascade process,[2,3] which has attracted enormous interest in the last decade. However, though it is simple in principle, it is not easy to implement experimentally. This is because of the existence of in-plane anisotropy in the QDs, the two biexciton decay pathways may have a small energy difference known as the fine structure splitting (FSS). When the FSS exceeds the radiative linewidth ($\sim 1.0\ \mu$eV), the polarization entanglement will be destroyed.[3,4] Great effort has been made to reduce the FSS using various post-growth tuning techniques.[5–13] Especially, it has recently been demonstrated that the FSS can be universally suppressed through the combination of electric field and stresses,[8,14] regardless of the dots' details.

In previous works, we have developed an effective model[13,14] based on symmetry analysis to explain how the FSS change under external stress. It turns out that the results obtained from the simple effective model is in excellent agreement with those obtained from a more sophisticated empirical pseudopotential method (EPM)[15] and configuration interaction (CI) calculations[16] and as well as the experimental results.[8,17,18] However, there is a hug gap between the effective model and the EPM calculations in understanding how exactly the strain modify the exciton coupling in the QDs at microscopic level.

The purpose of this paper is to bridge the gap between the effective model and the pseudopotential calculations. We derive analytically the exciton FSS under the external stresses in self-assembled InAs/GaAs QDs using the Bir-Pikus model.[19] We show that the strain induced valence bands mixing and valence-conduction bands (VB-CB) coupling play the most important roles in tuning the FSS. Detailed comparison between the Bir-Pikus model and the EPM calculations shows that the simple Bir-Pikus model provides semi-quantitatively description of the FSS under strain. We further clarify the polarization angle change under the external stresses.

The rest of paper is organized as follows. In Sec. II, we discuss how the single-particle states of a QD vary under the external stresses using the Bir-Pikus model. We discuss how the electron-hole exchange integrals and FSS change under the external stresses in Sec. III, and the exciton polarizations in Sec. IV. We summarize in Sec. V.

II. SINGLE-PARTICLE STATES IN A QD UNDER EXTERNAL STRAIN

We first look at how the single particle states in a QD vary under external strain field. Usually the applied uniaxial stress is less than ± 100 MPa. Under such small stress, the shape of QDs changes very little. We therefore neglect the change of envelope functions of the single particle states, and focus on the underlying atomistic wave functions. We further assume that dots have uniformly distributed strain due to the lattice mismatch between the InAs dot and GaAs matrix, and neglect the interface effects for the moment.

The influence of strain on valence states in zinc-blende structures can be described by the Bir-Pikus model.[19] We expand the Bir-Pikus Hamiltonian with in the six $|j, j_z\rangle$ states, i.e., heavy hole (HH) $|3/2, \pm 3/2\rangle$, light hole (LH) $|3/2, \pm 1/2\rangle$ and spin orbital (SO) $|1/2, \pm 1/2\rangle$ states, re-

sulting in the following 6×6 matrix,

$$\begin{pmatrix} P+Q & 0 & -\sqrt{2}S & R & S & \sqrt{2}R \\ 0 & P+Q & R^* & \sqrt{2}S^* & \sqrt{2}R^* & -S^* \\ -\sqrt{2}S^* & R & P-Q & 0 & \sqrt{2}Q & -\sqrt{3}S \\ R^* & \sqrt{2}S & 0 & P-Q & \sqrt{3}S^* & \sqrt{2}Q \\ S^* & \sqrt{2}R & \sqrt{2}Q & \sqrt{3}S & P & 0 \\ \sqrt{2}R^* & -S & -\sqrt{3}S^* & \sqrt{2}Q & 0 & P \end{pmatrix}, \tag{1}$$

where,

$$\begin{aligned} P &= a_v(e_{xx}+e_{yy}+e_{zz}), \\ Q &= \frac{b_v}{2}(e_{xx}+e_{yy}-2e_{zz}), \\ R &= \frac{\sqrt{3}}{2}b_v(e_{xx}-e_{yy}) - id_v e_{xy}, \\ S &= \frac{d_v}{\sqrt{2}}(e_{zx}-ie_{yz}). \end{aligned} \tag{2}$$

a_v, b_v, and d_v are the isotropic, biaxial, and shear deformation potentials respectively and e_{ij} are the strain components in the QDs. P describes the effects of isotropic hydrostatic strain and Q is associated with the biaxial strain. The effects of in-plane and off-plane strain anisotropy are accounted by R and S. In self-assembled InAs/GaAs QDs grown on the (001) GaAs substrate, the dot material is compressed in the growth plane and distended in the growth direction. We also consider the effects of strain anisotropy in the growth plane (e_{xy}, $e_{xx}-e_{yy}$) and off-plane shear strains (e_{zx} and e_{yz}).

For most III-V semiconductors, the SO bands are several hundreds meV below the HH and LH bands. The SO band were ignored in many previous works.[20–22] However, for self-assembled InGaAs/GaAs QDs and other nanostructures with large lattice mismatch, the biaxial strain is very large, which push the LH bands down towards the SO bands, therefore the coupling to the SO band is also important, as will be demonstrated in this work. Therefore, the full Hamiltonian should also includes the SO coupling term,

$$H_{\rm SO} = \frac{\Delta}{3}\begin{pmatrix} 1&0&0&0&0&0 \\ 0&1&0&0&0&0 \\ 0&0&1&0&0&0 \\ 0&0&0&1&0&0 \\ 0&0&0&0&-2&0 \\ 0&0&0&0&0&-2 \end{pmatrix}. \tag{3}$$

Here, $\Delta \sim 390$ meV is the SO parameter in InAs. The total Hamiltonian is given by $H = H_{\rm BP} + H_{\rm SO}$.

Because of the large lattice mismatch (7%) between InAs and GaAs in the InAs/GaAs QDs, the biaxial strain ($|e_{xx}+e_{yy}-2e_{zz}| \sim 24\%$) is much larger than the shear strains ($|e_{xx}-e_{yy}| \sim |e_{yz}| \sim |e_{zx}| \sim 1$ %, $|e_{xy}| \sim 0.5\%$). As a consequence, Q is comparable with the SO parameter Δ, much larger than $|R|$ and $|S|$. Therefore, we treat R and S as perturbations in the Hamiltonian. We calculate the first two (degenerate) hole states states up to second order of R and S,

$$\begin{aligned} \mathcal{N}|\psi_-^v\rangle = |\tfrac{3}{2},+\tfrac{3}{2}\rangle &+ \chi_\alpha|\tfrac{3}{2},+\tfrac{1}{2}\rangle + \chi_\beta|\tfrac{1}{2},+\tfrac{1}{2}\rangle \\ &+ \varepsilon_\alpha|\tfrac{3}{2},-\tfrac{1}{2}\rangle + \varepsilon_\beta|\tfrac{1}{2},-\tfrac{1}{2}\rangle, \\ \mathcal{N}|\psi_+^v\rangle = |\tfrac{3}{2},-\tfrac{3}{2}\rangle &+ \varepsilon_\alpha^*|\tfrac{3}{2},+\tfrac{1}{2}\rangle + \varepsilon_\beta^*|\tfrac{1}{2},+\tfrac{1}{2}\rangle \\ &- \chi_\alpha^*|\tfrac{3}{2},-\tfrac{1}{2}\rangle - \chi_\beta^*|\tfrac{1}{2},-\tfrac{1}{2}\rangle, \end{aligned} \tag{4}$$

where

$$\begin{aligned} \varepsilon_\alpha &= \frac{(3Q+\Delta)R^* + \sqrt{3}(S^*)^2}{2Q\Delta}, \\ \varepsilon_\beta &= \frac{3\sqrt{2}QR^* + \sqrt{6}(S^*)^2}{2Q\Delta}, \\ \chi_\alpha &= \frac{-\sqrt{2}\Delta S^* - \sqrt{6}SR^*}{2Q\Delta}, \\ \chi_\beta &= \frac{\sqrt{3}SR^*}{2Q\Delta}, \end{aligned} \tag{5}$$

and $\mathcal{N}^2 = 1 + |\varepsilon_\alpha|^2 + |\varepsilon_\beta|^2 + |\chi_\alpha|^2 + |\chi_\beta|^2 \sim 1$ is the normalization factor. The single-particle energy of the two states is,

$$\begin{aligned} E_v = P + Q + \frac{\Delta}{3} + \frac{2\Delta|S|^2 + (9Q+\Delta)|R|^2}{2Q\Delta} \\ + \frac{3\sqrt{3}(S^2R^* + (S^*)^2R)}{2Q\Delta}. \end{aligned} \tag{6}$$

These two states are still dominated by the HH ($j = 3/2$) states but mixing up with some LH and SO components. There are are two mixing mechanisms: (i) The mixing between HH and j_z states of the opposite signs is mainly due to the in-plane anisotropic strain effects or shape asymmetry (R). The mixing amplitude is determined by ε_α and ε_β. (ii) The mixing between HH and j_z states with the same sign is mainly due to the off-plane shear strain components (S). The mixing amplitude is determined by χ_α and χ_β. Both mixing mechanisms have important influence on the optical properties of the QDs, which will be discussed later in the paper.

For the simplicity of the discussion, we ignore the VB-CB coupling for a moment. But we will see later that the VB-CB coupling is also important for the FSS change under stain, which is addressed in the appendix. The Bloch parts of the conduction states are dominated by the lowest electron bands, $|\psi_+^c\rangle = |e\uparrow\rangle$ and $|\psi_-^v\rangle = |e\downarrow\rangle$. The energy of conduction states merely depends on hydrostatic strain:

$$\delta E_c(\overleftrightarrow{e}) = a_c(e_{xx}+e_{yy}+e_{zz}). \tag{7}$$

Under external stresses, the strain distribution in QDs changes accordingly, which changes the single-particle energy levels, as well as the coupling between the HH, LH and SO bands. We take the uniaxial stress along the [110] direction for example. The relation between the change

of strain and stress p along the [110] direction is given by,

$$\begin{aligned}\Delta e_{xx} &= \Delta e_{yy} = -\frac{1}{2}(S_{11}+S_{12})p\,,\\ \Delta e_{zz} &= -2S_{12}p\,,\\ \Delta e_{xy} &= -\frac{1}{4}S_{44}p\,,\\ \Delta e_{zx} &= \Delta e_{yz} = 0\,.\end{aligned} \tag{8}$$

Here, we take the compressive stress as positive one, and the parameters P, Q, R, S in the Bir-Pikus Hamiltonian under stress along the [110] direction can be written as,

$$\begin{aligned}P(p) &= P(0) - a_v(S_{11}+2S_{12})p\,,\\ Q(p) &= Q(0) - \frac{1}{2}b_v(S_{11}-S_{12})p\\ R(p) &= R(0) + i\frac{1}{4}d_v S_{44}p\\ S(p) &= S(0)\,.\end{aligned} \tag{9}$$

Interestingly, S does not change with the stress along the [110] direction. We have

$$\frac{dE_v}{dp} \approx -a_v(S_{11}+2S_{12}) - \frac{1}{2}b_v(S_{11}-S_{12})\,, \tag{10}$$

and

$$\frac{dE_c}{dp} = -a_c(S_{11}+2S_{12}). \tag{11}$$

Because the envelope functions of the electron and hole states change little, if the external stress is not very large, the direct electron-hole Coulomb interaction also change little. The change of the exciton energy is therefore mainly determined by the single-particle energies. We can estimate the of energy change to the stress along [110] direction as,

$$\frac{dE_{X^0}}{dp} \approx -(a_c-a_v)(S_{11}+2S_{12}) + \frac{1}{2}b_v(S_{11}-S_{12})\,. \tag{12}$$

Using the deformation potential parameters for bulk InAs material and elastic compliance constants for bulk GaAs material listed in Table I, we obtain $dE_{X^0}/dp \approx 12.3$ μeV/MPa. This value is in consistent with recent experimental results.[18] Although the exciton energy can be tuned by the stress along [110] direction, the tuning slope is rather small, because of the cancellation effect between the conduction band and valence bands in Eq. 12. Furthermore, in QDs the confinement potentials, alloy effects, etc. may also plays important roles to the exciton emission energies, therefore, dE_{X^0}/dp may vary from dots to dots.[18]

III. ELECTRON-HOLE EXCHANGE INTERACTION AND FSS

In this section we discuss how the external strain modifies the exciton exchange energies and the FSS. The matrix elements of the exciton Hamiltonian between different spin configurations is written as,[16]

$$\begin{aligned}\mathcal{H}_{v'c',vc} &= \langle\Phi_{v'c'}|\mathcal{H}|\Phi_{vc}\rangle\\ &= (E_c-E_v)\delta_{c,c'}\delta_{v,v'} - J_{v'c',vc} + K_{v'c',vc}\,,\end{aligned} \tag{13}$$

where the Js and Ks are the Coulomb and exchange integrals respectively. We consider only the first two hole states (ψ^v_+ and ψ^v_-) and electron states (ψ^c_+ and ψ^c_-). According to the symmetry, the only configurations with anti-parallel spins ($\psi^v_-\psi^c_+, \psi^v_+\psi^c_-$) make contributions to bright excitons (BE). In this basis, the many-particle

TABLE I. The compliance constants for GaAs and and deformation potentials for InAs. The deformation potentials for strained InAs is calculated by EPM using isotropic and biaxial strains for typical QDs.

Parameters	Unit	GaAs	InAs(bulk)[23]	InAs (strained)
a_c	eV	–	-5.08	–
a_v	eV	–	-1.0	-0.23
b_v	eV	–	-1.8	-2.22
d_v	eV	–	-3.6	-6.49
Δ	eV	–	0.39	0.33
S_{11}	10^{-2} GPa^{-1}	1.17		
S_{12}	10^{-2} GPa^{-1}	-0.37		
S_{44}	10^{-2} GPa^{-1}	1.68		

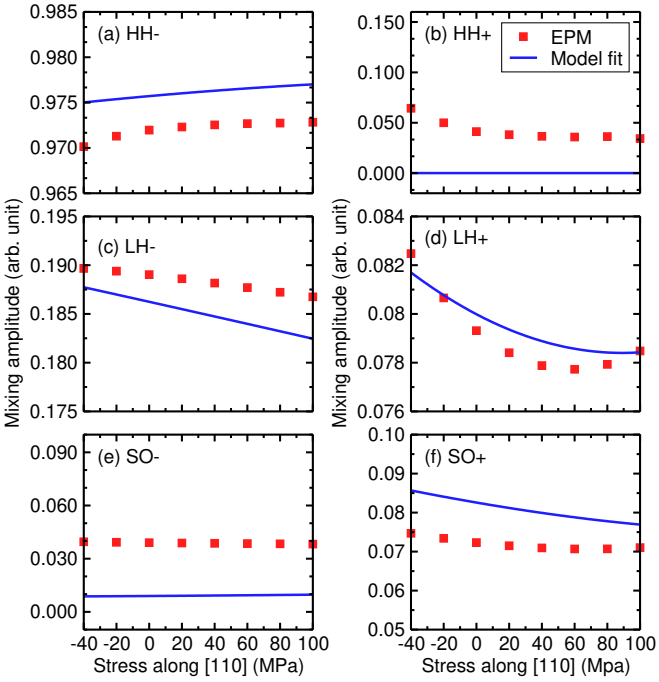


FIG. 1. (Color online) Valence bands mixing of the first hole state in a pure lens-shaped InAs/GaAs dot with base D=25 nm and height h=3.5 nm under uniaxial stress along the [110] direction, showing (a) HH$_+$, (b) HH$_-$, (c) LH$_+$, (d) LH$_-$, (e) SO$_+$ and (f) SO$_-$ components. The red squires are calculated from EPM, whereas the blue lines are obtained from Bir-Pikus model.

Hamiltonian for bright excitons is

$$H_{\rm BE} = (E_c - E_v) - J_{eh} + \begin{bmatrix} K_{\rm d} & K_{\rm od} \\ K_{\rm od}^* & K_{\rm d} \end{bmatrix}, \tag{14}$$

where J_{eh} is the electron-hole Coulomb interaction, $K_{\rm d}$ is the diagonal exchange energy, which determines the dark-bright exciton energy splitting, whereas the off-diagonal exchange energy,

$$\begin{aligned} K_{\rm od} &= \langle \psi_-^v \psi_+^c | \mathcal{K}_{\rm ex} | \psi_+^v \psi_-^c \rangle, \\ &= \iint \frac{[\psi_+^v(x_1)\psi_+^c(x_2)]^* \psi_-^c(x_1)\psi_-^v(x_2)}{\bar{\epsilon}(\mathbf{r}_1,\mathbf{r}_2)|\mathbf{r}_1 - \mathbf{r}_2|} dx_1 dx_2 \,, \end{aligned} \tag{15}$$

is responsible for the bright exciton energy splitting. After diagonalization of Eq. 14, the eigenstates of the two bright exciton can be written as,

$$|B_1\rangle = \frac{1}{\sqrt{2}}(|\psi_-^v \psi_+^c\rangle + {\rm e}^{i2\theta}|\psi_+^v \psi_-^c\rangle)\,, \tag{16}$$

$$|B_2\rangle = \frac{1}{\sqrt{2}}(|\psi_-^v \psi_+^c\rangle - {\rm e}^{i2\theta}|\psi_+^v \psi_-^c\rangle)\,, \tag{17}$$

with $2\theta = -\arg(K_{\rm od})$. The energy splitting between the two bright excitons, which is known as FSS, is given by $\Delta_{\rm FSS} = 2|K_{\rm od}|$. Let $a = (X + iY)/\sqrt{2}$ and $b = (X - iY)/\sqrt{2}$, and since only the hole and electron components of opposite spins in the same configuration have none-zero contribution to the exchange integral, the exchange integral can be written as (drop the spin index),

$$K_{\rm od} = \mathcal{N}^{-1}\langle (a + \varepsilon_+ b + \chi_- Z)e | \mathcal{K}_{ex} | (b + \varepsilon_+^* a + \chi_-^* Z)e \rangle \,, \tag{18}$$

with

$$\begin{aligned} \varepsilon_+ &= \frac{\varepsilon_\alpha + \sqrt{2}\varepsilon_\beta}{\sqrt{3}} = \frac{R^*}{2\sqrt{3}}\left(\frac{1}{Q} + \frac{9}{\Delta}\right) + \frac{3(S^*)^2}{2Q\Delta}\,, \\ \chi_- &= \frac{-\sqrt{2}\chi_\alpha + \chi_\beta}{\sqrt{3}} = \frac{S^*}{\sqrt{3}Q} + \frac{3SR^*}{2Q\Delta}\,. \end{aligned} \tag{19}$$

To simplify the notation, we introduce the following parameters,

$$\begin{aligned} \langle ae|\mathcal{K}_{ex}|ae\rangle \equiv \langle be|\mathcal{K}_{ex}|be\rangle &= K, \\ \langle ae|\mathcal{K}_{ex}|be\rangle &= \kappa + i\delta, \\ \langle ae|\mathcal{K}_{ex}|Ze\rangle \equiv \langle Ze|\mathcal{K}_{ex}|be\rangle &= \mu + i\nu, \\ \langle Ze|\mathcal{K}_{ex}|Ze\rangle &= K_z\,. \end{aligned} \tag{20}$$

Each parameter appearing in Eq. (20) can be expressed as exchange integrals over different orbital functions (X, Y, Z, S). For simplicity, we choose all orbital functions to be real. Therefore the parameters introduced here are all real. Exchange integrals over heavy holes $2K$ is approximately the dark-bright splitting, and

$$\kappa = \frac{1}{2}(\langle Xe|\mathcal{K}_{ex}|Xe\rangle - \langle Ye|\mathcal{K}_{ex}|Ye\rangle),$$

comes from the non-equivalence the orbital wave functions X and Y, whereas,

$$\delta = \frac{1}{2}(\langle Xe|\mathcal{K}_{ex}|Ye\rangle + \langle Ye|\mathcal{K}_{ex}|Xe\rangle)\,,$$

is due to the non-orthogonality between the orbital functions X, and Y. μ and ν is due to the non-orthogonality between the orbital functions X, Y to Z,

$$\begin{aligned} \mu &= \frac{1}{\sqrt{2}}\langle Xe|\mathcal{K}_{ex}|Ze\rangle\,, \\ \nu &= \frac{1}{\sqrt{2}}\langle Ye|\mathcal{K}_{ex}|Ze\rangle\,. \end{aligned} \tag{21}$$

With the above parameters, the whole exchange integral can be written as,

$$\begin{aligned} K_{\rm od} =& \frac{1}{\mathcal{N}}[(\kappa + i\delta) + 2\varepsilon_+ K + 2\chi_-(\mu + i\nu) \\ &+ 2\varepsilon_+\chi_-(\mu - i\nu) + \varepsilon_+^2(\kappa - i\delta) + \chi_-^2 K_z]\,. \end{aligned} \tag{22}$$

One can see clearly from Eq. (22), the origin of the FSS from the microscopic structure in the self-assembled QDs, apart from the dot shape asymmetry, including the non-orthogonality and non-equivalence between the atomic orbitals and the band mixing:

(i) For ideal QDs with D_{2d} and C_{4v} symmetry (e.g., a pure InAs/GaAs quantum disk), $e_{xx} - e_{yy}$=0, and e_{xy}, e_{yz}, e_{zx}=0, there is no coupling between HH with LH and SO bands, and κ, δ also vanish. There would be no FSS.

(ii) For QDs with C_{2v} symmetry (e.g., a pure lens-shaped InAs/GaAs QD), the orbital functions X and Y are of mirror symmetry about the [110] plane, therefore, $\kappa = 0$ and $\mu = \nu$. The strain distribution also obey such mirror symmetry, i.e., $e_{xx} = e_{yy}$, $e_{xy} \neq 0$, $e_{zx} = e_{yz} \neq 0$, as a result, $\varepsilon_+ = i|\varepsilon_+|$, $\chi_- = |\chi_-|e^{i\pi/4}$ [See Eq. (3) and Eq. (5)]. It is easy to verify that $K_{\rm od}$ is pure imaginary.

(iii) For a real dot with C_1 symmetry, $K_{\rm od}$ has both a real part and an imaginary part.

Because $|\varepsilon_+|$,$|\chi_-| \ll 1$, and κ, δ, μ, $\nu \ll K$, K_z, $K_{\rm od}$ can be further approximated as $K_{\rm od} \approx (\kappa + i\delta) + 2\varepsilon_+ K$. We assume that the parameters introduced in Eq. (20) associated with the atomistic orbitals of the underlying dot materials will not change under small external stress. Therefore the change of the exchange integral (away from the critical stress region[13]) can be written as,

$$\frac{dK_{\rm od}}{dp} \approx 2\frac{d\varepsilon_+}{dp}K\,. \tag{23}$$

Using Eq. 9 and Eq. 19, we have,

$$\frac{d\varepsilon_+}{dp} \approx \frac{1}{2\sqrt{3}}\left(\frac{1}{Q} + \frac{9}{\Delta}\right)\frac{dR^*}{dp}\,. \tag{24}$$

Here, we neglect the change of Q in the denominator. For stress applied along the [110] direction,

$$\frac{dR^*}{dp} = -i\frac{1}{4}d_v S_{44}. \tag{25}$$

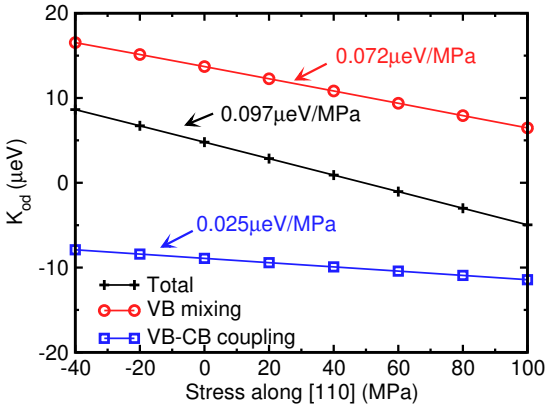


FIG. 2. (Color online) The off-diagonal electron-hole exchange interactions $|K_{\rm od}|$ in a lens-shaped InAs/GaAs QD (D= 25 nm, h= 3.5 nm) as functions of the uniaxial stress along the [110] direction. The black line is the total $|K_{\rm od}|$, whereas the red and blue lines are the contribution from VB mixing and VB-CB coupling respectively.

Therefore, we have the $K_{\rm od}$ change under the stress along [110] direction,

$$\frac{dK_{\rm od}}{dp} \approx -i\left(\frac{9Q+\Delta}{4\sqrt{3}Q\Delta}\right) d_v S_{44} K\,. \qquad (26)$$

Using parameters given in Table I, we get $d\varepsilon_+/dp = i\,2.455\times10^{-4}{\rm MPa}^{-1}$. In typical InAs/GaAs QDs, the exciton dark-bright splitting is approximately $2K \sim 200\mu$eV. Therefore we estimate that $d\Delta_{\rm FSS}/dp \sim 0.1$ μeV/MPa, which is in the same order of magnitude with the experimental values[24] of $(0.34\pm0.08)\mu$eV/MPa. As shown in the appendix, the VB-CB coupling also contribute to the change FSS in a similar magnitude.

Interestingly, as one can see from Eq. (24-26) that stress along the [110] direction only changes the imaginary part of the exchange integral $K_{\rm od}$, which is just the α parameter defined in Ref. 13. It is also easy to verify that stress along the [100] or [010] direction only changes the real part of the exchange integral $K_{\rm od}$, which is β defined in Ref. 13. (Note that the basis of exciton wave function in Eq. 14 is different than that used in Ref. 13). For dots with C_{2v} symmetry, in which $K_{\rm od}$ has only an imaginary part, the stress along the [110] direction alone can tune the FSS to zero, whereas for dots with C_1 symmetry, in which $K_{\rm od}$ has both a real part and an imaginary part, the FSS cannot be tuned to zero under single uniaxial stress. However, since the stresses along the [110] and [100] directions can manipulate the imaginary and real parts of $K_{\rm od}$ (almost) independently, the FSS can be tuned to nearly zero, as predicted in our previous work.[14]

Of course the above Bir-Pikus model is highly simplified. The real QDs are far more complicated. To see if this model is valid, we perform EPM calculations on realistic InAs/GaAs QDs under external stresses. The dots are assumed to be grown on the [001] direction and embedded in a $60\times60\times60$ GaAs supercell. The atom positions in the supercell are optimized by the valence force field method.[25,26] We solve the single-particle states by expanding the wavefunctions with a strained linear combination of Bloch bands method (SLCBB).[27] The exciton energies are calculated by the CI method,[16] in which the exciton wavefunctions are expanded in Slater determinants constructed from all confined electron and hole single-particle states.

To compare with the Bir-Pikus model, we project the first hole single-particle wave function to the $|j, j_z\rangle$ states at Γ point.[28] The results are shown in Fig. 1, compared with those from model calculations. The solid squares represent the amplitude of different components obtained from empirical pseudopotentials calculations by integrating the envelop functions of each component over the whole supercell. The blue lines are the results obtained from Bir-Pikus model, using deformation potentials for strained InAs given in Table I. The wave functions are normalized to 1 in both cases. We see that the EPM and Bir-Pikus model results are in a reasonable good agreement with each other (Note that the scale of the figure is extremely small). In the Bir-Pikus model, HH_+ and HH_- components do not mix with each other, whereas in the EPM calculations, there is small mixing of HH_+ and HH_- states, because the SLCBB method use Bloch basis functions from many k-points around the Γ point, whereas the Bir-Pikus model[19] use only the Bloch basis functions at Γ point. Importantly the highly simplified Bir-Pikus model gives similar slopes of the magnitude of the components to the external stress as those from atomistic calculations. The quantitative differences between the two theories are due to the neglect of the nonuniform distribution of strain, inter-facial effects, etc. in the Bir-Pikus model.

We further compare the exchange integrals $K_{\rm od}$ between the two theories. Figure 2 depicts the EPM calculated exchange integral $K_{\rm od}$ in a pure lens-shaped InAs/GaAs QD with base D=25 nm and height h=3.5 nm as a function of the stress along the [110] direction. The total $K_{\rm od}$ under external stress, shown in black line, is 0.097 μeV/MPa, and the change of FSS under stress is $2K_{\rm od}$=0.192 μeV/MPa. We can decompose the change of $K_{\rm od}$ into the contributions from valence bands mixing (red line), and the VB-CB coupling (blue line). The EPM calculated contribution due to valence bands mixing is 0.072 μeV/MPa, compared with 0.049 μeV/MPa from the 6×6 Bir-Pikus model, and the EPM calculated contribution from VB-CB coupling is 0.025 μeV/MPa compared with 0.036 μeV/MPa from the 8x8 model Bir-Pikus model discussed in the Appendix.

It is quite surprising that the highly simplified Bir-Pikus model could catch the change of FSS under external strain rather well, especially, it is known that the $k\cdot p$ theory greatly underestimates the FSS in the QDs.[29] The reason is as follows. The absolute values of FSS are determined by the combined effects of the strain distributions, alloy, interfacial effects etc., which can not be captured

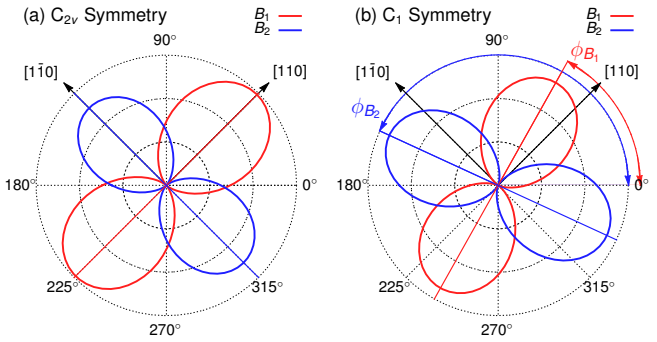


FIG. 3. (Color online) Schematic plot of polar diagrams of (a) dot with C_{2v} symmetry and (b) dot with C_1 symmetry.

well by the continuum theories. However, these atomistic effects do not change much if the applied external stress is not too large. On the other hand, the underlying crystal structure and electronic structure change coherently under the applied external stress which break explicitly the C_{4v} symmetry of the system. Therefore, we expect that the *change* of the FSS under stress can be capture rather well by the Bir-Pikus model, even though the absolute vale of the FSS could be dramatically underestimated.

IV. EXCITON POLARIZATION ANGLE

We now discuss the polarization properties of the two bright exctions using the above Bir-Pikus model. The transition dipole matrix elements are given by,

$$\mathcal{M} = \langle 0|\hat{\mathbf{n}}\cdot\mathbf{r}|\Psi_X\rangle\,, \tag{27}$$

where $\hat{\mathbf{n}}$ is the polarization vector, and Ψ_X is the exciton wave function, which is obtained by diagonalize Eq. 14. The emission intensities of the two bright excitons, passing through a linear polarizer with an angle α with respect to the [100] axis are given by,[22]

$$\begin{aligned} I_{B_1}(\alpha) &= I_0[\cos(\theta+\alpha) + |\varepsilon_+|\cos(\theta+\phi_\varepsilon-\alpha)]^2\,,\\ I_{B_2}(\alpha) &= I_0[\sin(\theta+\alpha) + |\varepsilon_+|\sin(\theta+\phi_\varepsilon-\alpha)]^2\,, \end{aligned} \tag{28}$$

with $\phi_\varepsilon = \arg(\varepsilon_+)$, whereas $2\theta = -\arg(K_{\rm od})$ is the argument of $K_{\rm od}$, as shown in Fig. 3. Eq. 28 is similar to the one proposed by Tonin et. al.,[22] however, the interpretation to the equations is very different. In Ref. 22, θ is the main elongation axis orientation with respect to [1$\bar{1}$0] determined by the growing process, which would not change under the external strain. In our model, the polarization angle θ is determined by the argument of $K_{\rm od}$. When stress modifies the exchange integral $K_{\rm od}$ and its argument, the exciton states rotate in the x-y plane accordingly, consistent with the effective model proposed by the authors in Ref. 13.

In the presence of band mixing ε_+, the angle between the two states in the x-y plane will deviate from $\pi/2$ slightly. The polarization angle between the two bright exciton states in the x-y plane is,

$$\begin{aligned} \Delta\phi = |\phi_{B_2} - \phi_{B_1}| &= \frac{\pi}{2} + \arctan\left[-\frac{2|\varepsilon_+|\sin(2\theta+\phi_\varepsilon)}{1-|\varepsilon_+|^2}\right]\\ &= \frac{\pi}{2} - 2\sin[(2\theta+\phi_\varepsilon)]|\varepsilon_+| + O(|\varepsilon_+|^3)\,. \end{aligned} \tag{29}$$

For dots with C_{2v} symmetry, we have $\phi_\varepsilon = 2\theta = \frac{\pi}{2}$ according to the analysis in Sec. III, and therefore $\Delta\phi = \frac{\pi}{2}$. The two emission lines are perpendicular to each other in the x-y plane and aligned in the [110] and [1$\bar{1}$0] directions respectively [See Figure 3 (a)]. This is still true when the dots are under stress along the [110] direction. For dot with C_1 symmetry, we have $e_{xx} \neq e_{yy}$ and $e_{zx} \neq e_{yz}$. Therefore ϕ_ε and 2θ will deviate from $\frac{\pi}{2}$. The polarization angles of the two emission lines are,

$$\begin{aligned} \phi_{B_1} &= \arctan\left[-\frac{\sin\theta + |\varepsilon_+|\sin(\theta+\phi_\varepsilon)}{\cos\theta - |\varepsilon_+|\cos(\theta+\phi_\varepsilon)}\right]\\ &= -\theta - \sin[(2\theta+\phi_\varepsilon)]|\varepsilon_+| + O(|\varepsilon_+|^2)\,, \end{aligned} \tag{30}$$

and

$$\begin{aligned} \phi_{B_2} &= \arctan\left[\frac{\cos\theta + |\varepsilon_+|\sin(\theta+\phi_\varepsilon)}{\sin\theta - |\varepsilon_+|\cos(\theta+\phi_\varepsilon)}\right]\\ &= \frac{\pi}{2} - \theta + \sin[(2\theta+\phi_\varepsilon)]|\varepsilon_+| + O(|\varepsilon_+|^2)\,, \end{aligned} \tag{31}$$

with respect to [100] direction [See Figure 3 (b)]. In this case, $\Delta\phi \neq \pi/2$, and the magnitude of the deviation is proportional to the band mixing parameter ε_+.

V. SUMMARY

We derive analytically the exciton fine structure splitting under the external stress in the self-assembled InAs/GaAs quantum dots using the Bir-Pikus model. We find that the FSS change is mainly due to the strain induced valence bands mixing and valence-conduction band coupling. The polarization angle change under strain is due to the change of the complex phase of the electron-hole off-diagonal exchange integrals. The derived theory agrees well with the effective theory and the empirical pseudopotential calculations, and therefore bridge the gap between the two theories.

ACKNOWLEDGMENTS

LH acknowledges the support from the Chinese National Fundamental Research Program 2011CB921200, and the National Natural Science Funds for Distinguished Young Scholars.

Appendix A: 8×8 Bir-Pikus model

In the main text of the paper, we neglect the coupling between conduction band (CB) and valence bands (VB).

To include the the VB-CB coupling, we shall use a 8×8 model Hamiltonian in the basis set of (e+, e-, HH+, HH-, LH+, LH-, SO+, SO-),

$$H=\begin{pmatrix} E_g+G & 0 & \sqrt{3}T & 0 & -\sqrt{2}W & T^* & W & \sqrt{2}T^* \\ 0 & E_g+G & 0 & \sqrt{3}T^* & T & \sqrt{2}W & \sqrt{2}T & -W \\ \sqrt{3}T^* & 0 & P+Q+\frac{\Delta}{3} & 0 & -\sqrt{2}S & R & S & \sqrt{2}R \\ 0 & \sqrt{3}T & 0 & p+Q+\frac{\Delta}{3} & R^* & \sqrt{2}S^* & \sqrt{2}R^* & -S^* \\ -\sqrt{2}W & T^* & -\sqrt{2}S^* & R & P-Q+\frac{\Delta}{3} & 0 & \sqrt{2}Q & -\sqrt{3}S \\ T & \sqrt{2}W & R^* & \sqrt{2}S & 0 & P-Q+\frac{\Delta}{3} & \sqrt{3}S^* & \sqrt{2}Q \\ W & \sqrt{2}T^* & S^* & \sqrt{2}R & \sqrt{2}Q & \sqrt{3}S & P-\frac{2\Delta}{3} & 0 \\ \sqrt{2}T & -W & \sqrt{2}R^* & -S & -\sqrt{3}S^* & \sqrt{2}Q & 0 & P-\frac{2\Delta}{3} \end{pmatrix}, \tag{A1}$$

where P, Q, R, S are defined in Eq. 9 in the main text. The parameters G, W and T describe the VB-CB coupling,

$$\begin{aligned} G &= a_c(e_{xx}+e_{yy}+e_{zz})\,, \\ W &= d_c e_{xy}\,, \\ T &= \frac{d_c}{\sqrt{2}}(e_{yz}+ie_{zx}). \end{aligned} \tag{A2}$$

We treat R, S, W and T as perturbations in the Hamiltonian and solve the eigenvectors up to the second order of these parameters. The obtained hole wave functions are,

$$\begin{aligned} |\psi^v_-\rangle =& \tfrac{1}{N_v}[|\mathrm{hh}+\rangle+\chi_\alpha|\mathrm{lh}+\rangle+\chi_\beta|\mathrm{so}+\rangle+\varepsilon_\alpha|\mathrm{lh}-\rangle \\ &+\varepsilon_\beta|\mathrm{so}-\rangle+\eta_\alpha|\mathrm{S}+\rangle+\eta_\beta|\mathrm{S}-\rangle] \\ |\psi^v_+\rangle =& \tfrac{1}{N_v}[|\mathrm{hh}-\rangle+\varepsilon^*_\alpha|\mathrm{lh}+\rangle+\varepsilon^*_\beta|\mathrm{so}+\rangle-\chi^*_\alpha|\mathrm{lh}-\rangle \\ &-\chi^*_\beta|\mathrm{so}-\rangle-\eta^*_\beta|\mathrm{S}+\rangle+\eta^*_\alpha|\mathrm{S}-\rangle]\,, \end{aligned} \tag{A3}$$

with

$$N_v=\sqrt{1+|\varepsilon_\alpha|^2+|\varepsilon_\beta|^2+|\chi_\alpha|^2+|\chi_\beta|^2+|\eta_\alpha|^2+|\eta_\beta|^2}\,. \tag{A4}$$

The electron wave functions are,

$$\begin{aligned} |\psi^c_+\rangle =& \tfrac{1}{N_c}[|\mathrm{S}+\rangle+\tau^*_\alpha|\mathrm{hh}+\rangle+\tau^*_\beta|\mathrm{hh}-\rangle+\lambda^*_\alpha|\mathrm{lh}+\rangle \\ &+\lambda^*_\beta|\mathrm{so}+\rangle+l^*_\alpha|\mathrm{lh}-\rangle+l^*_\beta|\mathrm{so}-\rangle]\,, \\ |\psi^c_-\rangle =& \tfrac{1}{N_c}[|\mathrm{S}-\rangle-\tau_\beta|\mathrm{hh}+\rangle+\tau_\alpha|\mathrm{hh}-\rangle+l_\alpha|\mathrm{lh}+\rangle \\ &+l_\beta|\mathrm{so}+\rangle-\lambda_\alpha|\mathrm{lh}-\rangle-\lambda_\beta|\mathrm{so}-\rangle]\,, \end{aligned} \tag{A5}$$

with

$$N_c=\sqrt{1+|\tau_\alpha|^2+|\tau_\beta|^2+|\lambda_\alpha|^2+|\lambda_\beta|^2+|l_\alpha|^2+|l_\beta|^2}\,. \tag{A6}$$

Define $a=(X+iY)/\sqrt{2}$ and $b=(X-iY)/\sqrt{2}$, and ignore the normalization factors, we have,

$$\begin{aligned} |\psi^v_-\rangle &= |(a+\varepsilon_+ b+\chi_- Z+\eta_\alpha S)\uparrow+(\chi_+ a+\varepsilon_- Z+\eta_\beta S)\downarrow\rangle\,, \\ |\psi^c_+\rangle &= |(S+\tau^*_\alpha a+l^*_+ b+\lambda^*_- Z)\uparrow+(\tau^*_\beta b+\lambda^*_+ a+l^*_- Z)\downarrow\rangle\,, \\ |\psi^v_+\rangle &= |(b+\varepsilon^*_+ a+\chi^*_- Z+\eta_\beta S)\downarrow-(\chi^*_+ b+\varepsilon^*_- Z+\eta_\beta S)\uparrow\rangle\,, \\ |\psi^c_-\rangle &= |(S+\tau_\alpha b+l_+ a+\lambda_- Z)\downarrow-(\tau_\beta a+\lambda_+ b+l_- Z)\uparrow\rangle\,, \end{aligned} \tag{A7}$$

where

$$\begin{aligned} \varepsilon_+ &= \frac{\varepsilon_\alpha+\sqrt{2}\varepsilon_\beta}{\sqrt{3}}\,, \quad \varepsilon_- = \frac{\sqrt{2}\varepsilon_\alpha-\varepsilon_\beta}{\sqrt{3}}\,, \\ \chi_+ &= \frac{\chi_\alpha+\sqrt{2}\chi_\beta}{\sqrt{3}}\,, \quad \chi_- = \frac{-\sqrt{2}\chi_\alpha+\chi_\beta}{\sqrt{3}}\,, \\ l_+ &= \frac{l_\alpha+\sqrt{2}l_\beta}{\sqrt{3}}\,, \quad l_- = \frac{\sqrt{2}l_\alpha-l_\beta}{\sqrt{3}}\,. \\ \lambda_+ &= \frac{\lambda_\alpha+\sqrt{2}\lambda_\beta}{\sqrt{3}}\,, \quad \lambda_- = \frac{-\sqrt{2}\lambda_\alpha+\lambda_\beta}{\sqrt{3}}\,, \end{aligned} \tag{A8}$$

The exchange integral between configurations $|\psi_-^v\psi_+^c\rangle$ and $|\psi_+^v\psi_-^c\rangle$

$$\begin{aligned}
K_{\rm od} =&\langle\psi_-^v\psi_+^c|\mathcal{K}_{\rm ex}|\psi_+^v\psi_-^c\rangle\\
=&\frac{1}{N_c^2N_v^2}(\langle a\uparrow S\uparrow|\mathcal{K}_{\rm ex}|b\downarrow S\downarrow\rangle\\
&+\varepsilon_+\langle b\uparrow S\uparrow|\mathcal{K}_{\rm ex}|b\downarrow S\downarrow\rangle\\
&+\varepsilon_+\langle a\uparrow S\uparrow|\mathcal{K}_{\rm ex}|a\downarrow S\downarrow\rangle\\
&+\varepsilon_+^2\langle b\uparrow S\uparrow|\mathcal{K}_{\rm ex}|a\downarrow S\downarrow\rangle\\
&+\chi_-\langle Z\uparrow S\uparrow|\mathcal{K}_{\rm ex}|b\downarrow S\downarrow\rangle\\
&+\chi_-\langle a\uparrow S\uparrow|\mathcal{K}_{\rm ex}|Z\downarrow S\downarrow\rangle\\
&+\chi_-^2\langle Z\uparrow S\uparrow|\mathcal{K}_{\rm ex}|Z\downarrow S\downarrow\rangle\\
&+\varepsilon_+\chi_-\langle b\uparrow S\uparrow|\mathcal{K}_{\rm ex}|Z\downarrow S\downarrow\rangle\\
&+\varepsilon_+\chi_-\langle Z\uparrow S\uparrow|\mathcal{K}_{\rm ex}|a\downarrow S\downarrow\rangle\\
&+\tau_\alpha^2\langle a\uparrow a\uparrow|\mathcal{K}_{\rm ex}|b\downarrow b\downarrow\rangle\\
&+\eta_\alpha^2\langle S\uparrow S\uparrow|\mathcal{K}_{\rm ex}|S\downarrow S\downarrow\rangle\\
&+\eta_\alpha\tau_\alpha\langle a\uparrow a\uparrow|\mathcal{K}_{\rm ex}|S\downarrow S\downarrow\rangle\\
&+\eta_\alpha\tau_\alpha\langle S\uparrow S\uparrow|\mathcal{K}_{\rm ex}|b\downarrow b\downarrow\rangle\\
&+\varepsilon_+l_+\tau_\alpha\langle a\uparrow a\uparrow|\mathcal{K}_{\rm ex}|a\downarrow a\downarrow\rangle\\
&+\varepsilon_+l_+\tau_\alpha\langle b\uparrow b\uparrow|\mathcal{K}_{\rm ex}|b\downarrow b\downarrow\rangle\\
&+\varepsilon_+l_+\eta_\alpha\langle b\uparrow b\uparrow|\mathcal{K}_{\rm ex}|S\downarrow S\downarrow\rangle\\
&+\varepsilon_+l_+\eta_\alpha\langle S\uparrow S\uparrow|\mathcal{K}_{\rm ex}|a\downarrow a\downarrow\rangle\\
&+\chi_-\lambda_-\tau_\alpha\langle Z\uparrow Z\uparrow|\mathcal{K}_{\rm ex}|a\downarrow a\downarrow\rangle\\
&+\chi_-\lambda_-\tau_\alpha\langle b\uparrow b\uparrow|\mathcal{K}_{\rm ex}|Z\downarrow Z\downarrow\rangle\\
&+\chi_-\lambda_-\eta_\alpha\langle Z\uparrow Z\uparrow|\mathcal{K}_{\rm ex}|S\downarrow S\downarrow\rangle\\
&+\chi_-\lambda_-\eta_\alpha\langle S\uparrow S\uparrow|\mathcal{K}_{\rm ex}|Z\downarrow Z\downarrow\rangle\\
&+(\varepsilon_+l_+)^2\langle b\uparrow b\uparrow|\mathcal{K}_{\rm ex}|a\downarrow a\downarrow\rangle\\
&+(\chi_-\lambda_-)^2\langle Z\uparrow Z\uparrow|\mathcal{K}_{\rm ex}|Z\downarrow Z\downarrow\rangle\\
&+\ldots)
\end{aligned}\tag{A9}$$

There are 1024 terms in total in Eq. A9, and we list only important terms. If there is no band mixing, e.g., in the dots with C_{4v} and above symmetry, only the first term in Eq. (A9) exists, which is exact zero for the high symmetry dots as discussed in the main text. If we consider only the valence bands mixing (the 6x6 model in the main text of the paper), only the first 9 terms in Eq. (A9) exist. Other terms are due to VB-CB coupling. Because in the InAs/GaAs QDs, the hole-hole Coulomb interactions $J_{\rm hh}=\langle h\uparrow h\uparrow|\mathcal{K}_{\rm ex}|h\downarrow h\downarrow\rangle$ are very close to the electron-electron Coulomb interactions $J_{\rm ee}=\langle e\uparrow e\uparrow|\mathcal{K}_{\rm ex}|e\downarrow e\downarrow\rangle$ and electron-hole Coulomb interactions $J_{\rm eh}=\langle e\uparrow e\uparrow|\mathcal{K}_{\rm ex}|h\downarrow h\downarrow\rangle$, where h=a or b or Z, are the hole orbitals and $e=S$ is the electron orbital, we can simplify Eq. (A9) as

$$\begin{aligned}
K_{\rm od} =&\frac{1}{N_c^2N_v^2}[(\kappa+i\delta)+2\varepsilon_+K+2\chi_-(\mu+i\nu)\\
&+2\varepsilon_+\chi_-(\mu-i\nu)+\varepsilon_+^2(\kappa-i\delta)+\chi_-^2K_z\\
&+(\varepsilon_+l_++\chi_-\lambda_-+\tau_\alpha)^2J_{\rm hh}\\
&+2(\varepsilon_+l_++\chi_-\lambda_-+\tau_\alpha)\eta_\alpha J_{\rm eh}\\
&+\eta_\alpha^2J_{\rm ee}+\ldots]
\end{aligned}\tag{A10}$$

In typical InAs/GaAs QD, $J_{\rm ee}\approx J_{\rm eh}\approx J_{\rm hh}\overset{\rm def}{=}J$. Additionally $|\varepsilon_+|,|\chi_-|,l_+,\lambda\ll1$, and $\kappa,\delta,\mu,\nu\ll K,K_z\ll J$, therefore $K_{\rm od}$ can be further simplified as,

$$K_{\rm od}\approx(\kappa+i\delta)+2\varepsilon_+K+(\varepsilon_+l_++\chi_-\lambda_-+\tau_\alpha+\eta_\alpha)^2J\tag{A11}$$

The first two terms in the above equation has been obtained from the 6×6 model, whereas the last term is due to VB-CB coupling. As we shall see later, though the VB-CB coupling is much weaker than the valence bands mixing, the contribution to the FSS change is still significant, because $J\sim20$ meV is much larger than $K\sim100$ μeV. Therefore, we keep higher order terms of VB-CB band mixing.

Let us denote $E_g'=E_g+G-P-Q-\Delta/3$ and $E_g''=E_g+G-P+2Q+2\Delta/3$, where $E_g\approx1$ eV is the single-particle band gap of the strained InAs. After tedious but straightforward derivation, we have,

$$\tau_\alpha+\eta_\alpha\approx0\,,\tag{A12}$$

$$\varepsilon_+\approx\frac{(9Q+\Delta)R^*}{2\sqrt{3}Q\Delta}\,,\tag{A13}$$

$$l_+\approx\frac{\sqrt{3}T^*}{E_g'}\,,\tag{A14}$$

$$\chi_-\approx\frac{S^*}{\sqrt{3}Q}\,,\tag{A15}$$

$$\lambda_-\approx\frac{\sqrt{3}W}{E_g''}\,.\tag{A16}$$

Here we have used the fact that $E_g'\sim E_g''\gg Q,\,\Delta$. By using the relationship $W=i(R-R^*)d_c/(2d_v)$ and $T=iSd_c/d_v$, we obtain,

$$\begin{aligned}
&\varepsilon_+l_++\chi_-\lambda_-+\tau_\alpha+\eta_\alpha\\
\approx&i\frac{d_c}{d_v}\frac{S^*}{2Q}\left[\frac{R-R^*}{E_g''}-\frac{R^*}{E'}\left(\frac{9Q}{\Delta}+1\right)\right]
\end{aligned}\tag{A17}$$

It is easy to show that $d(\tau_\alpha+\eta_\alpha)/dp$, dl_+/dp, $d\chi_-/dp$, $d\lambda_-/dp\ll d\varepsilon_+/dp$, which has been obtained in Eq. 24. For the stress along the [110] direction, we have

$$\begin{aligned}
\frac{dK_{\rm od}}{dp}\approx&2\frac{d\varepsilon_+}{dp}K+2(\varepsilon_+l_++\chi_-\lambda_-+\tau_\alpha+\eta_\alpha)l_+\frac{d\varepsilon_+}{dp}J\\
\approx&-i\frac{9Q+\Delta}{4\sqrt{3}Q\Delta}d_vS_{44}K\\
&+i\frac{1}{8}\left(\frac{d_c}{d_v}\frac{S^*}{E_g'}\frac{9Q+\Delta}{Q\Delta}\right)^2R^*d_vS_{44}J\,,
\end{aligned}\tag{A18}$$

where the first term has been obtained from the 6×6 model in the main text, and the second term is due to the VB-CB coupling. In typical InAs/GaAs QDs, $E_g' \sim 1$ eV and $E_g'' \sim 2$ eV, $Q \sim 0.23$ eV, $\Delta \sim 0.34$ eV and $|S| \sim 0.065$ eV. The electron-hole Coulomb interactions $J \sim 20$ meV, and dark-bright splitting energy $2K \sim 200$ μeV. Using the parameters given in Table I, we have $d\varepsilon_+/dp \approx i2.4 \times 10^{-4}$ MPa^{-1}. Finally, we obtain $dK_{\rm od}/dp \approx i(0.049 + 0.036) = i0.084$ μeV/MPa, which is in a reasonable good agreement with the EPM calculations and the experimental values.

* helx@ustc.edu.cn.

[1] D. Bimberg, M. Grundmann, and N. N. Ledentsov, Quantum Dot Heterostructures (John Wiley & Sons, 1999).
[2] O. Benson, C. Santori, M. Pelton, and Y. Yamamoto, Phys. Rev. Lett. **84**, 2513 (2000).
[3] R. M. Stevenson, R. J. Young, P. Atkinson, K. Cooper, D. A. Ritchie, and A. J. Shields, Nature **439**, 179 (2006).
[4] M. Gong, K. Duan, C. F. Li, R. Magri, G. A. Narvaez, and L. He, Phys. Rev. B **77**, 045326 (2008).
[5] A. J. Bennett, M. A. Pooley, R. M. Stevenson, M. B. Ward, R. B. Patel, A. Boyer de la Giroday, N. Sköld, I. Farrer, C. A. Nicoll, D. A. Ritchie, et al., Nature Phys. **6**, 947 (2010).
[6] B. D. Gerardot, S. Seidl, P. A. Dalgarno, R. J. Warburton, D. Granados, J. M. Garcia, K. Kowalik, O. Krebs, K. Karrai, A. Badolato, et al., Appl. Phys. Lett. **90**, 041101 (2007).
[7] M. M. Vogel, S. M. Ulrich, R. Hafenbrak, P. Michler, L. Wang, A. Rastelli, and O. G. Schmidt, Appl. Phys. Lett. **91**, 051904 (2007).
[8] R. Trotta, E. Zallo, C. Ortix, P. Atkinson, J. D. Plumhof, J. van den Brink, A. Rastelli, and O. G. Schmidt, Phys. Rev. Lett. **109**, 147401 (2012).
[9] F. Ding, R. Singh, J. D. Plumhof, T. Zander, V. Křápek, Y. H. Chen, M. Benyoucef, V. Zwiller, K. Dörr, G. Bester, et al., Phys. Rev. Lett. **104**, 067405 (2010).
[10] K. D. Jöns, R. Hafenbrak, R. Singh, F. Ding, J. D. Plumhof, A. Rastelli, O. G. Schmidt, G. Bester, and P. Michler, Phys. Rev. Lett. **107**, 217402 (2011).
[11] S. Seidl, M. Kroner, A. Högele, K. Karrai, R. J. Warburton, A. Badolato, and P. M. Petroff, Appl. Phys. Lett. **88**, 203113 (2006).
[12] X. M. Dou, B. Q. Sun, B. R. Wang, S. S. Ma, R. Zhou, S. S. Huang, H. Q. Ni, and Z. C. Niu, Chin. Phys. Lett. **25**, 1120 (2008).
[13] M. Gong, W. Zhang, G.-C. Guo, and L. He, Phys. Rev. Lett. **106**, 227401 (2011).
[14] J. Wang, M. Gong, G.-C. Guo, and L. He, Applied Physics Letters **101**, 063114 (2012).
[15] A. J. Williamson, L.-W. Wang, and A. Zunger, Phys. Rev. B **62**, 12963 (2000).
[16] A. Franceschetti, H. Fu, L.-W. Wang, and A. Zunger, Phys. Rev. B **60**, 1819 (1999).
[17] J. D. Plumhof, V. Křápek, F. Ding, K. D. Jöns, R. Hafenbrak, P. Klenovský, A. Herklotz, K. Dörr, P. Michler, A. Rastelli, et al., Phys. Rev. B **83**, 121302 (2011).
[18] C. E. Kuklewicz, R. N. E. Malein, P. M. Petroff, and B. D. Gerardot, Nano Lett. **12**, 3761 (2012).
[19] G. E. Pikus and G. L. Bir, Fiz. Tverd. Tela (Leningrad) **1**, 154, (1959); **1**, 1642 (1959); **3**, 1001 (1961) [Sov. Phys. Solid State **1**, 136 (1959); **1**, 1502 (1959); **3**, 730 (1961)]; Phys. Rev. Lett. **6**, 103 (1961).
[20] Y. Léger, L. Besombes, L. Maingault, and H. Mariette, Phys. Rev. B **76**, 045331 (2007).
[21] C. Testelin, F. Bernardot, B. Eble, and M. Chamarro, Phys. Rev. B **79**, 195440 (2009).
[22] C. Tonin, R. Hostein, V. Voliotis, R. Grousson, A. Lemaitre, and A. Martinez, Phys. Rev. B **85**, 155303 (2012).
[23] I. Vurgaftman, J. R. Meyer, and L. R. Ram-Mohan, J. of Appl. Phys. **89**, 5815 (2001).
[24] S. Seidl, M. Kroner, A. Hogele, K. Karrai, R. J. Warburton, A. Badolato, and P. M. Petroff, Appl. Phys. Lett. **88**, 203113 (2006).
[25] P. N. Keating, Phys. Rev **145**, 637 (1966).
[26] R. Martin, Phys. Rev. B **1**, 4005 (1970).
[27] L.-W. Wang and A. Zunger, Phys. Rev. B **59**, 15806 (1999).
[28] H. Wei, M. Gong, G.-C. Guo, and L. He, Phys. Rev. B **85**, 045317 (2012).
[29] R. Seguin, A. Schliwa, S. Rodt, K. Pötschke, U. W. Pohl, and D. Bimberg, Phys. Rev. Lett. **95**, 257402 (2005).